Available online at www.sciencedirect.com
ScienceDirect
Journal of Magnetic Resonance 185 (2007) 270–282
JMR Journal of Magnetic Resonance
www.elsevier.com/locate/jmr

Dynamic phase shifts in nanoscale distance measurements by double electron electron resonance (DEER) ☆

Michael K. Bowman [a,*], Alexander G. Maryasov [b]

[a] *Structural Biology and Microimaging, Battelle Northwest, Richland, WA 99354, USA*
[b] *Institute of Chemical Kinetics and Combustion, Siberian Branch of the Russian Academy of Sciences, Novosibirsk 630090, Russia*

Received 28 October 2006; revised 8 December 2006
Available online 22 December 2006

Abstract

The off-resonant pump pulse used in double electron electron resonance (DEER) measurements produces dynamic phase shifts that are explained here by simple analytic and vector descriptions of the full range of signal behaviors observed during DEER measurements, including: large phase shifts in the signal; changes in the position and shape of the detected echo; and changes in the signal intensity. The dynamic phase shifts depend on the width, amplitude and offset frequency of the pump pulse. Isolated radicals as well as pairs or clusters of dipolar-coupled radicals have the same dynamic phase shift that is independent of pump pulse delay in a typical measurement. A method of calibrating both the pump pulse offset frequency and the pump pulse field strength is outlined. A vector model is presented that explains the dynamic phase shifts in terms of precessing magnetization that is either spin locked or precessing about the effective pump field during the pump pulse. Implications of the dynamic phase shifts are discussed as they relate to setting up, calibrating and interpreting the results of DEER measurements.

Keywords: DEER; PELDOR; Double electron electron resonance; Electron electron double resonance

1. Introduction

The measurement of nanoscale distances in the range of 2–8 or more nanometers between free radicals or other paramagnetic centers has become practical using a technique known as double electron electron resonance (DEER) or pulsed electron electron double resonance (PELDOR) [1–4]. The method involves the measurement of the frequency shift in one free radical caused by the change in the magnetic dipolar interaction when a second free radical is perturbed by a 'pump' pulse of a different microwave frequency. The signal is detected as an electron spin echo, which has the advantage of refocusing and eliminating static, inhomogeneous broadening while revealing only dynamic events resulting from the 'pump' microwave pulse.

It is widely assumed that the pump pulse width, frequency, and intensity can be readily adjusted so that the pump pulse has no direct effect on the observed echo signal and has only an indirect effect mediated by the dipolar coupling to a second free radical more in 'resonance' with the pump pulse frequency. This is clearly not the case. It has long been known both in magnetic resonance and in quantum optics that off-resonance fields do affect both the frequency and phase of all spectral lines. We find that these off-resonant field effects are easily observed under typical conditions for DEER measurements and provide a convenient method for calibrating the frequency and the amplitude of the pump field.

☆ This manuscript has been authored by Battelle Memorial Institute, Pacific Northwest Division, under Contract No. DE-AC05-76RL0 1830 with the US Department of Energy. The United States Government retains and the publisher, by accepting the article for publication, acknowledges that the United States Government retains a non-exclusive, paid-up, irrevocable, world-wide license to publish or reproduce the published form of this manuscript, or allow others to do so, for United States Government purposes.

* Corresponding author. Fax: +1 509 376 2303.
E-mail address: michael.bowman@pnl.gov (M.K. Bowman).

1090-7807/$ - see front matter © 2007 Elsevier Inc. All rights reserved.
doi:10.1016/j.jmr.2006.12.011

In 1940, Bloch and Siegert examined the effect of the counter-rotating circularly polarized component of the linearly polarized field on a magnetic resonance spectrum [5]. They considered the frequency, ω_2, which is the negative of the Larmor frequency, *i.e.*, $\omega_2 = -\omega_0 = -\gamma B_0$. They found that the magnetic resonance lines were shifted to higher field by $B_2^2/4B_0$, an amount "which however in all practical cases is negligibly small" [5]. Fifteen years later Ramsey described the more general case of fields at arbitrary frequencies [6]. He reached two important conclusions that are very relevant for DEER: (1) the shift in the line position becomes quite large for a nearly resonant field and (2) the off-resonant field is effective even as a short pulse applied during the excitation or the measurement of the magnetic resonance signal. The effect of off-resonant fields has been considered in many contexts and under many different names, for instance, as spin decoupling in NMR; as dynamic Stark splitting or light shift in quantum optics [7]; as transient Bloch–Siegert phases or shifts in ENDOR [8], NMR [9] and multiquantum magnetic resonance [10]; and as dressed states in dynamic nuclear polarization [11]. Most treatments have sought limiting expressions for the size of the shift in an experimental context far from that of DEER and none describes the full range of effects from off-resonant fields that we observe in DEER measurements.

We have developed simple analytic and vector descriptions of the dynamic phase shifts caused by the off-resonant field that do describe the full range of signal behaviors observed during DEER measurements, including: large phase shifts in the signal; changes in the position and shape of the detected echo; and changes in the intensity. These are dynamic effects that originate during the pump pulse but persist through the observation of the EPR signal. These effects provide a simple means of calibrating the frequency and the amplitude of the pumping field while setting up a DEER measurement that may prove particularly useful in high-frequency EPR DEER measurements. The effect of the pumping field on the detected spins can be confused with the desired DEER response and must be considered while setting up and interpreting DEER measurements.

We start by calculating the effect of an off-resonant microwave pulse in a typical DEER measurement. The calculations are then compared to experimental signals from isolated free radicals. The calibration of the DEER pumping frequency and amplitude is described and a simple vector model is presented.

2. Results

2.1. Effect of off-resonant fields

We first consider a set of isolated, non-interacting electron spins and focus on an EPR transition between a single pair of levels. We assume that the transition as well as the pumping and observation EPR frequencies are well separated from all other transitions so that the spins can be treated as an effective $S = 1/2$ system. Later, we briefly consider interacting spins and multiple level systems. We consider oscillating microwave fields that are separated in time as did Ramsey [6], but we focus on the sample magnetization rather than the eigenfunctions. We make no approximations concerning the magnitudes of the fields. We ignore the counter-rotating components of the fields that are the source of the classic Bloch–Siegert shift [5] because they have such large resonance offsets that their effect on the signal is negligible compared to other terms.

The prototypical DEER measurement [12] is made using the spin echo double resonance (SEDOR) pulse sequence illustrated in Fig. 1. The initial spin magnetization M_z is converted by one or more microwave pulses at an 'observation' frequency ω_0 into precessing magnetization M_x and M_y. After some time, a pump pulse at a frequency of $\omega_0 - \Delta$ is applied followed later by another pulse at ω_0. The difference between the frequencies of the 'observation' and pump pulse is Δ. The magnetization evolves until it rephases to form the spin echo which is the detected signal. In the simplest sequences, the positions of the observation frequency pulses are fixed in time while the position of the pump pulse is swept within the first precession period. In the DEER measurement, the purpose of the pump pulse is to cause an electron spin flip in a radical that has a small dipolar coupling to an observed spin. This shifts the precession frequency of the observed spin by the dipolar interaction, modulating the amplitude of the observed spin echo and allowing measurement of the dipolar interaction.

For calculating the dynamic phase shifts, we find it convenient to use a rotating frame at the pump frequency but with the x and y axes referenced initially to the microwave fields at ω_0. The pump and observe frequencies are incoherent with each other, so that there is no specific phase

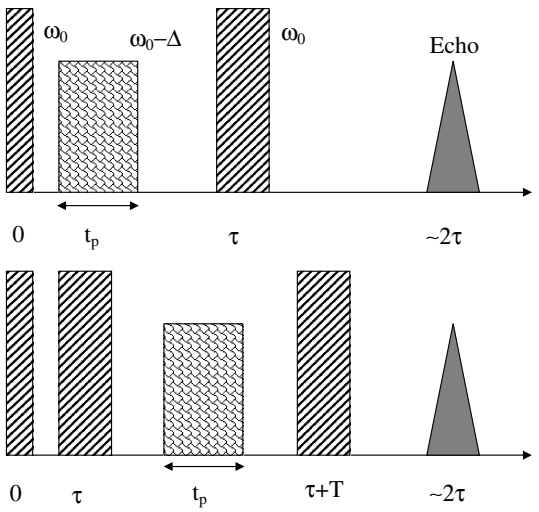

Fig. 1. Pulse sequences for three pulse DEER, upper, and four pulse DEER, lower. The 'observe' microwave pulses are indicated by diagonal hatching to distinguish them from the 'pump' pulse at a different frequency. The approximate location of the detected echo signal is indicated by the triangle.

relation between the pump field B_2 and our chosen rotating frame. We will call the angle between them β. The effective field in this rotating frame for an observed spin is given by the vector $\vec{\Omega}_{\text{eff}} = (\gamma B_2 \cos(\beta), \gamma B_2 \sin(\beta), \Delta + \delta)$ during the pump pulse and (0, 0, $\Delta + \delta$) when no pulses are present. The resonance offset of the spin packet from the 'observation' frequency, ω_0, is δ. The magnetization following a pump pulse with duration t is

$$\vec{M}(t) = \vec{M}(0)\cos(\Omega_{\text{eff}}t) + \frac{\vec{\Omega}_{\text{eff}}}{\Omega_{\text{eff}}^2}(\vec{M}(0)\cdot\vec{\Omega}_{\text{eff}})(1-\cos(\Omega_{\text{eff}}t)) + \frac{\vec{\Omega}_{\text{eff}}\otimes\vec{M}(0)}{\Omega_{\text{eff}}}\sin(\Omega_{\text{eff}}t) \quad (1)$$

where $\Omega_{\text{eff}} = |\vec{\Omega}_{\text{eff}}|$. The only spins that contribute to the detected electron spin echo are ones which have precessing magnetization both before and after the pump pulse. This fact greatly simplifies our calculations by limiting the number and type of coherence pathways that must be considered.

At the start of the pump pulse, an arbitrary spin packet will have a phase, α, relative to the rotating frame that depends on δ and the time delay before the pump pulse. Strictly speaking, $\vec{M}(0) = (\cos(\alpha), \sin(\alpha), 0)$ but we can take $\vec{M}(0) = (1,0,0)$ without loss of generality because the phase, α, is refocused during the formation of the detected electron spin echo. The dependence of the observed signal on the random phase, β, between $\vec{M}(0)$ and $\vec{\Omega}_{\text{eff}}$ in Eq. (1) is eliminated by signal averaging over the course of a measurement. This is fortunate for two reasons. (1) It means that the averaged effect of the pump field is independent of the position of the pump pulse in the precession period of the DEER measurement, so that the dynamic phase shift does not vary as the position of the pump pulse is changed during a DEER measurement. (2) It avoids the need to keep track of α, β, and the offset frequencies. Consequently, we can use the simplest model of a DEER sequence with only two pulses at ω_0 and with the pump pulse immediately following the first ω_0 pulse and obtain results that are valid for the four-pulse and even more elaborate DEER pulse sequences. At the end of the pump pulse, the parts of Eq. (1) that contribute to the detected signal, after averaging over all possible values of β, reduce to

$$M_+(t_p) = M_x(t_p) + iM_y(t_p) = \frac{\gamma^2B_2^2 + \left(2(\Delta+\delta)^2 + \gamma^2B_2^2\right)\cos\left[t_p\sqrt{(\Delta+\delta)^2+\gamma^2B_2^2}\right]}{2\left((\Delta+\delta)^2+\gamma^2B_2^2\right)} + i\frac{(\Delta+\delta)\sin\left[t_p\sqrt{(\Delta+\delta)^2+\gamma^2B_2^2}\right]}{\sqrt{(\Delta+\delta)^2+\gamma^2B_2^2}} \quad (2)$$

This magnetization precesses at a rate corresponding to the operator $\exp[it(\Delta+\delta)S_z]$ until the second observation frequency pulse and then to the operator $\exp[-it(\Delta+\delta)S_z]$ until an echo forms and the signal is detected. The effect of the pump pulse is easily seen by calculating the precession to the nominal center of the echo and then taking the ratio of the magnetization with and without the pump pulse:

$$M_{\text{Rel}} = \frac{M_+(t_p)}{M_+(0)}e^{-it_p(\Delta+\delta)} = M_+(t_p)e^{-it_p(\Delta+\delta)} = e^{-it_p(\Delta+\delta)}\left(A + B\cos\left[t_p\sqrt{(\Delta+\delta)^2+\gamma^2B_2^2}\right] + iC\sin\left[t_p\sqrt{(\Delta+\delta)^2+\gamma^2B_2^2}\right]\right) \quad (3)$$

where $A = \gamma^2B_2^2/\{2\Omega_{\text{eff}}^2\}$, $B = 1 - A$, and $C = (\Delta+\delta)/\Omega_{\text{eff}}$. Eq. (3) can be expanded into

$$M_{\text{Rel}} = A\exp\left[-it_p(\Delta+\delta)\right] + \frac{B-C}{2}\times\exp\left[-it_p(\Delta+\delta+\Omega_{\text{eff}})\right] + \frac{B+C}{2}\times\exp\left[-it_p(\Delta+\delta-\Omega_{\text{eff}})\right] \quad (4)$$

There are three distinct terms with different amplitudes and different dependences on the experimental parameters. The first term, with coefficient A, represents a phase shift in the signal. The term in the exponential of $t_p\Delta$ is independent of resonance offset of the spin packet (δ) and produces an overall phase shift in the echo that depends on the difference, Δ, between microwave frequencies. The term $t_p\delta$ is a linear phase shift proportional to the resonance offset of the spin packet. Such a linear phase shift produces a shift in the position of the echo peak, that is, the time when the phases of all spin packets refocus. The time shift in the echo maximum is simply t_p, with the echo appearing sooner than in the absence of the pump pulse. Thus, the first term produces an echo advanced in time by the t_p and phase shifted by $t_p\Delta$. The inhomogeneous broadening δ is effectively turned off during the pump pulse for the first term in Eq. (4) so that it dephases only for a time $\sim\tau - t_p$, rather than for τ.

The second and third terms are similar, but the phase shifts include Ω_{eff}, the effective field during the pump pulse. If the pump amplitude is small compared to its frequency offset, then $\Omega_{\text{eff}} \sim \Delta + \delta$ and the second term produces an echo with roughly twice the phase shift and advanced by $\sim 2t_p$ while the third term produces an echo that is not greatly shifted in either time or phase. On the other hand, when the offset is small compared to the pump field, $\Omega_{\text{eff}} \sim \gamma B_2$, both echoes are advanced in time by t_p and in addition to a phase shift of $t_p\Delta$, the amplitudes are modulated by $\cos^2(1/2\,\Omega_{\text{eff}}t_p)$. The amplitudes and frequencies (in the exponential) of all three terms continue smoothly through $\Delta + \delta = 0$ with curves **1** in Fig. 2 continuing as **1** while **2** and **3** interchange. The frequencies ω are positive or negative as required by the terms in the exponentials of Eq. (4). The same dynamic phase shift effects occur when the pump pulse lies between the second observation

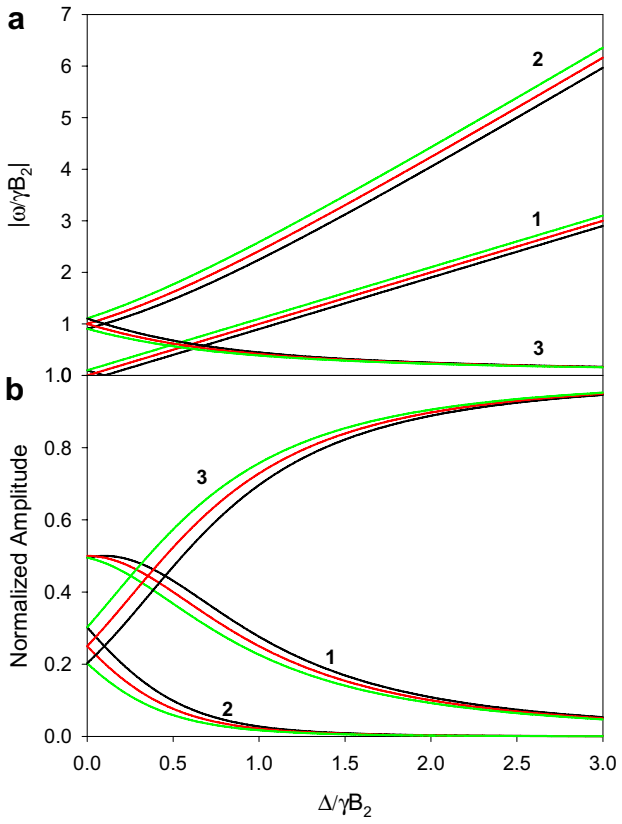

Fig. 2. The frequencies, **A**, and the amplitudes, **B**, of the three terms in Eq. (4), see text. The red curves correspond to $\delta = 0$, while the green and black curves correspond to $\delta = \pm 0.1\ \gamma B_2$, respectively. (For interpretation of the references to color in this figure legend, the reader is referred to the web version of this paper.)

frequency pulse and the echo, except that the phase shifts have opposite sign and the echoes are delayed rather than advanced in time.

Although t_p is kept constant in a DEER measurement, it is useful to consider what would happen if t_p were varied. Instead of considering the phase shift ωt_p, we examine the frequency ω, which is the rate of change of phase. The frequencies of the three terms in Eq. (4) are plotted as a function of the pump frequency offset Δ in Fig. 2a. The first, or 'A', term indicated in the figure by the set of curves **1**, depends on $-(\Delta + \delta)$, the sum of the pump offset and the offset of the spin packet from the observation frequency. The two flanking lines for curve **1** for $\delta = \pm 0.1\gamma B_2$ show that the frequency for the first term is equal to $\Delta + \delta$ for all values of $\Delta/\gamma B_2$, producing a shift in the peak of the spin echo for the first term by exactly t_p. For broad lines, the integral of the contribution from the first term in Eq. (4) to the echo evolves at exactly Δ. This part of the signal provides a convenient experimental measure of Δ. The amplitude of this signal is shown in Fig. 2b as the set of curves **1**. For very large Δ, the amplitude falls off as $\gamma^2 B_2^2/\Delta^2$ but gives a measurable signal at the frequency Δ for typical DEER measurements.

The second and third terms in Eq. (4) evolve at frequencies of $-(\Delta + \delta \pm \Omega_{\text{eff}})$, respectively, curves **2** and **3** in Fig. 2a. The dependence of the second frequency on δ is nearly linear, between 1δ and 2δ, producing a shift in the echo ranging between t_p and $2t_p$. This second term can be difficult to observe because its normalized amplitude falls off as $\gamma^4 B_2^4/8\Delta^4$ and is only 2% of the total signal when $\gamma B_2 = \Delta$. The amplitude of the third term, on the other hand, approaches $1 - \gamma^2 B_2^2/\Delta^2$ for large Δ while its frequency approaches $\gamma^2 B_2^2/(2\Delta)$ and its echo is only slightly shifted in time by $\gamma^2 B_2^2/\Delta^2 t_p$.

If echoes corresponding to the three terms in Eq. (4) are measured using a fairly broad integrator gate as t_p is progressively increased, the measured signal will arise largely from those spin packets with $\delta \sim 0$, as illustrated in the Appendix. Thus, γB_2 is readily obtained from the difference in frequencies measured for the first and third terms using

$$\begin{aligned} &|\Delta - (\Delta \pm \Omega_{\text{eff}})| = \Omega_{\text{eff}} \\ &\sqrt{\Omega_{\text{eff}}^2 - \Delta^2} = \gamma B_2 \end{aligned} \tag{5}$$

or from the second and third terms using

$$\sqrt{|(\Delta + \Omega_{\text{eff}})(\Delta - \Omega_{\text{eff}})|} = \gamma B_2 \tag{6}$$

and can be used to adjust the pulse width and amplitude for DEER measurements.

Echoes corresponding to the three terms in Eq. (4) are often resolved for t_p larger than the width of the unperturbed spin echo which is roughly t'_p, the width of the ω_0 pulses. However, in the typical DEER measurement, t_p is comparable to or smaller than t'_p so that the three terms in Eq. (4) are unresolved. Because they are modulated at different frequencies by the dynamic phase shifts, the signals from the three terms interfere with each other, resulting in a signal that not only has a net phase shift, but also has reduced intensity. This effect is illustrated in Fig. 3, where the magnitude as well as the real and imaginary parts of the echo are plotted for $t_p \ll t'_p$ with $\gamma B_2 t_p = \pi$. It is obvious from the two quadrature components of the signal that significant dynamic phase shifts occur even for large offsets, Δ. The total echo magnitude is reduced except when $|\Delta/\gamma B_2| = \sqrt{4n-1}$ for n any integer greater than zero with $\gamma B_2 t_p = \pi$. Analogous phase and amplitude changes occur for any value of t_p, and the corresponding magnitude maxima are located at $|\Delta/\gamma B_2| = \sqrt{4n - \gamma B_2 t_p/\pi}$. The echo signal disappears for $\Delta = 0$ in Fig. 3 because the phase, β, of the pumping field relative to the field at ω_0 is random so that the pump pulse with $\gamma B_2 t_p = \pi$ randomizes the phase of all magnetization that otherwise would form the spin echo signal.

2.2. Spin echo shapes

The two quadrature components of the electron spin echo from γ-irradiated sugar at room temperature (with $\Delta/\gamma B_2 = (2\pi\ 61.2\ \text{MHz})/(2\pi\ 55.3\ \text{MHz}) = 1.12$ as calculated from the parameters measured below) are shown in Fig. 4 for several different pumping pulse widths. The echo clearly splits as predicted into three echoes, each with a

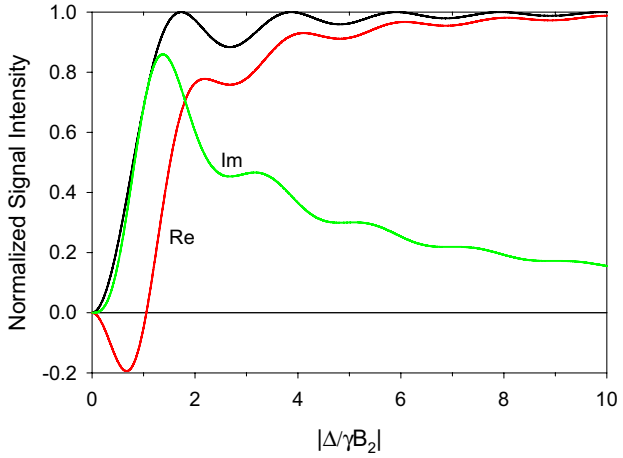

Fig. 3. The amplitudes of the real and imaginary quadrature components (red and green, respectively) and the magnitude (black) of the detected DEER echo as a function of the normalized offset frequency, Δ, for $\gamma B_2 t_p = \pi$ and $\delta = 0$, assuming that the three components of the echo are unresolved. (For interpretation of the references to color in this figure legend, the reader is referred to the web version of this paper.)

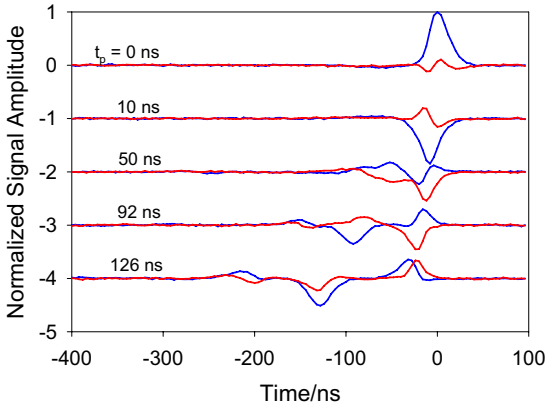

Fig. 4. The detected DEER echo from γ-irradiated sugar measured for various values of t_p at room temperature using a three pulse DEER sequence with $\Delta/(2\pi) = 61.2$ MHz and $\gamma B_2/(2\pi) = 55.3$ MHz. The blue ad red traces are the real and imaginary components of the quadrature echo signal. For large values of t_p, the echo is resolved into the three components, with different phase dependences, described by Eq. (4). (For interpretation of the references to color in this figure legend, the reader is referred to the web version of this paper.)

different phase, appearing at times separated by approximately t_p. These are taken from the 2D plot in Fig. 5 where the positions of the three echoes and the frequencies at which their phases evolve are clearly seen.

There is a series of alternating positive and negative bands running at a 45° angle across Fig. 5. This is the signal from the first term in Eq. (4) and its amplitude is modulated by $\Delta/2\pi = 61.3$ MHz as t_p increases. Its intensity increases noticeably with increasing t_p because the effective 'τ' for this spin echo is decreased by $\sim t_p$ and the echo has decreasingly less time to decay as t_p increases.

Another prominent band runs nearly vertically and corresponds to the third term in Eq. (4). Its initial amplitude is quite large, as expected from Fig. 2b at $\Delta/\gamma B_2 = 1.12$, but

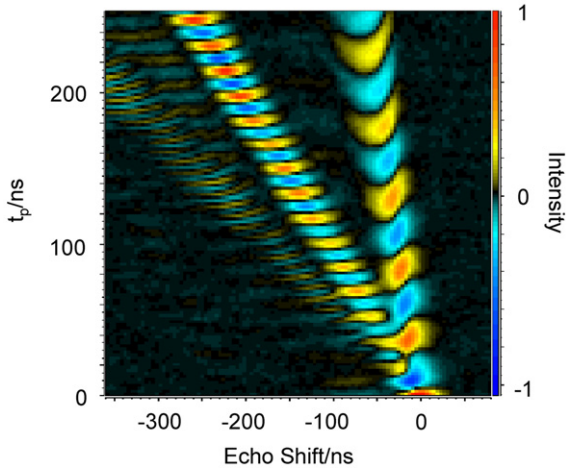

Fig. 5. Two-dimensional, time-domain spectrum showing echo intensity as a function of pump pulse width. Same conditions as Fig. 4.

diminishes as t_p increases. The distribution of B_2 along the length of the sample in the resonator causes this decay and also produces some curvature in the bands at large t_p. The intensity of this echo is modulated at a frequency of -21.2 MHz when the quadrature signal channel is taken into consideration. This frequency corresponds to $\Delta - \Omega_{eff}$, giving $\Omega_{eff}/2\pi = 82.5$ MHz and a calculated value of $\gamma B_2/2\pi = 55.3$ MHz. The echo from the second term in Eq. (4) is also visible as a weak signal shifted by somewhat less than $2t_p$ in Figs. 4 and 5. Its intensity is modulated at 143.8 MHz which agrees with the value calculated for $\Delta + \Omega_{eff}$.

2.3. Variation with Δ

The observed spin echo showed similar behavior for other values of Δ and B_2. For large Δ and t_p, the echo split into three well-resolved peaks separated by t_p as in Fig. 4. For small Δ, the peaks were not resolved and the entire echo was advanced by t_p. The frequencies modulating the echo intensity are easily measured by either summing (projecting) the 2D time-domain signals in Fig. 5 onto the t_p axis or by integrating the signal over a window comparable to the horizontal axis of Fig. 5, followed by Fourier transformation. If the two quadrature channels of data are retained, the positive and negative frequencies corresponding to terms in Eq. (4) appear. The frequencies and fields strengths measured over a range of Δ are summarized in Table 1. There is a discrepancy of $\sim$2% between the 'set' and 'measured' values of $|\Delta|$ that is an instrumental artifact discussed in the Appendix.

The observed frequencies are in quantitative agreement with Eq. (4). The maximum γB_2 occurs for $\Delta = 0$, the nominal resonant frequency of the split ring resonator. Both the peak value of γB_2 and its variation with Δ depend strongly on the amount of over-coupling of the resonator. Pumping fields are quite useful for DEER even beyond $\Delta/2\pi = \pm 120$ MHz in the strongly over-coupled resonator used here, Fig. 6.

Table 1
Pump fields measured from dynamic phase shifts

$\Delta/2\pi$ Set	$\Delta/2\pi$ Term **1**	$(\Omega_{eff}+\Delta)/2\pi$ Term **2**	$(-\Omega_{eff}+\Delta)/2\pi$ Term **3**	$\Omega_{eff}/2\pi$	$\gamma B_2/2\pi$
120.0	122.3		−6.4	128.7	40.1
100.0	101.9		−10.9	112.8	48.4
80.0	81.5		−16.2	97.7	53.9
60.0	61.2	151.9	−27.6	88.8	64.3
40.0	40.8	133.8	−51.1	91.9	82.3
20.0	20.4		−88.6	109.0	107.1
0.0	0.0	108.8	−108.4	108.6	108.6
−20.0	−20.3	65.1	−105.8	85.4	83.0
−40.0	−40.6	29.8	−112.1	70.4	57.5
−50.0	−50.8	20.0	−122.4	70.8	49.3
−60.0	−61.1	13.8	−137.0	74.9	43.3
−80.0	−81.4	8.9		90.3	39.1
−100.0	−101.8	5.1		106.9	32.6
−120.0	−122.1	2.4		124.5	24.3

The frequencies measured as t_p is incremented are assigned to terms in Eq. (4). $\Delta/2\pi$ as set by the spectrometer software is reported in the first column. Ω_{eff} and γB_2 are derived using Eq. (5) using Term **2** or Term **3** with the smallest magnitude. γB_2 derived from Eq. (6) differed by less than 1%. Data were measured at 344 mT with $\omega_0/2\pi = 9627.3$ MHz. The observing pulse lengths were 8 and 16 ns separated by 600 ns using the MPFU channels and correspond to turning angles of $\pi/2$ and π, respectively. The pump pulse was placed 40 ns after the first observe pulse with t_p incremented in 2 ns steps at the maximum power from an SPFU channel. Each quadrature signal channel was integrated over a 500 ns window ending just after the spin echo in the absence of a pump pulse. The integral as a function of t_p was apodized with a half-sine-bell and zero-filled to 8 K followed by complex Fourier Transformation. The frequencies of peaks in the absolute value spectrum are reported and have not been multiplied by 0.982 to correct for the effects of capacitive loading described in the Appendix.

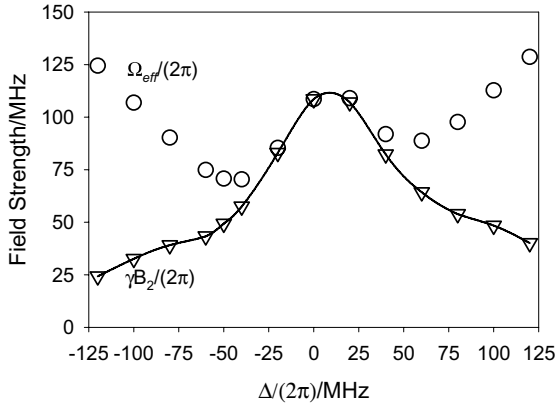

Fig. 6. The effective field, Ω_{eff}, (open circles) and the microwave pump field, γB_2, (inverted triangles) derived using Eq. (5) are plotted versus Δ, the offset between the pump and observing frequencies. Data were measured at 344 mT with $\omega_0/2\pi = 9627.3$ MHz. The observing pulse lengths were 8 and 16 ns separated by 600 ns using the MPFU channels and correspond to turning angles of $\pi/2$ and π, respectively. Maximum pump pulse power was used with attenuator settings of 0 dB starting 40 ns after the first observe pulse and t_p was incremented in 2 ns steps. The echoes in each quadrature signal channel were integrated over a 500 ns window ending just after the spin echo in the absence of a pump pulse. The integral as a function of t_p was apodized with a half-sine-bell and the 256 points zero-filled to 8 K followed by complex Fourier Transformation. The derived field strengths have not been multiplied by 0.982 to correct for the effects of capacitive loading described in the Appendix.

2.4. A vector model

The effect of an off-resonant pumping pulse on the detected spin echo signal in the context of a DEER measurement can be explained by a simple vector model. Fig. 7a shows the rotating frame at the pumping frequency $\omega_0 - \Delta$ following the first microwave pulse at ω_0 just prior to the pump pulse. Purely for convenience, we now take the X and Y axes in the rotating frame to be defined by the B_2 field. The green arrow in the XY plane is the magnetization of an arbitrary spin packet which we will follow. The red arrow directed along the Z-axis is the local effective field experienced by that spin packet in the rotating frame, $\Delta + \delta$. The spin packet magnetization has no consistent phase relationship to the rotating coordinate system because it was prepared with an ω_0 pulse that is not coherent with the pump field. The spin packet can be oriented anywhere in the XY plane as represented by the yellow disk, so we will arbitrarily choose the phase of the green arrow to simplify discussion. When a large pump field is applied along the X-axis of the rotating frame, the effective field is tilted to some position in the XZ plane, Fig. 7b, at an angle determined by $\Delta + \delta$ and γB_2. Spin packets with different δ will have effective fields with different magnitudes and direction. The spin packet magnetization precesses in the cone shown in yellow around the new effective field. At this point, it is convenient to split the spin packet magnetization in Fig. 7b into a component parallel and a component perpendicular to the effective field, shown in Fig. 7c and d, respectively.

The component parallel (or antiparallel) to the effective field has no net force acting on it in the rotating frame, so it is stationary or 'spin-locked', Fig. 7c, except for its slow decay at a rate of $1/T_{1\rho}$. At the end of the pump pulse, the effective field returns to the Z axis and the spin-locked magnetization precesses in a cone around it. The projection of the magnetization onto the XY plane, Fig. 7e, helps form

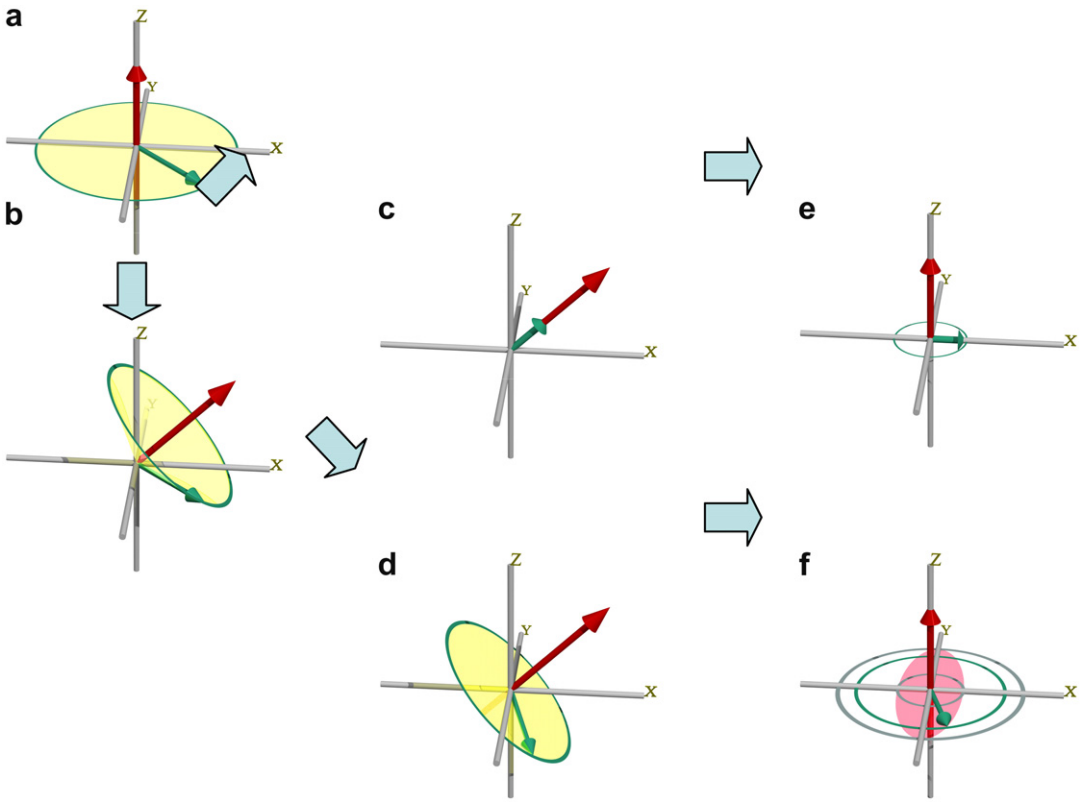

Fig. 7. A vector model to explain the origin of the echoes and frequencies found in the DEER echo. See text for detailed description.

the detected spin echo signal, but the projection along the Z axis does not. This spin locked signal is the first term in Eq. (4) and undergoes no motion that depends on the magnitude of the effective field.

The perpendicular component precesses at a rate of Ω_{eff} in the plane perpendicular to the effective field and tilted with respect to the XY plane, Fig. 7d. The magnetization traces out the tilted yellow circle. When the pump pulse ends and the effective field returns to the Z-axis, the circle is projected back onto the XY plane as an ellipse with the major axis along Y and the minor axis along X. Only the magnetization in an ellipse on the XY plane, shown in pink in Fig. 7f, contributes to the detected spin echo; the magnetization that ends up parallel to the Z-axis does not. The pink ellipse merely indicates the intensity of the magnetization that is initially mapped back onto the XY plane. Each magnetization vector precesses in a circle, for instance the one drawn in green traces out the green circle. The larger and smaller vectors which would appear along the Y and X axes, respectively, trace out the larger and smaller light blue circles. The spin echo signal from this perpendicular component of the magnetization forms the second and third terms in Eq. (4).

But how does magnetization precessing at the single rate of Ω_{eff} around the effective field during the pump pulse produce two signals with distinctly different dependences on t_{p}? It is quite clear that the magnetization rotates at one rate and in one direction around the effective field in Fig. 7d. Yet, before detection, it is projected back onto the ellipse in Fig. 7f and, as t_{p} increases, the magnetization varies from a large projection along the Y-axis to a smaller projection along the X-axis and back along Y. The projection from the tilted plane produces an amplitude modulation, in effect, elliptical polarization in the XY plane. The periodic variation in the amount of magnetization that gets projected onto the XY plane can be represented as the sum of two counter-rotating components at $\pm\Omega_{\text{eff}}$ but with different amplitudes. These two counter-rotating components then combine with the rotating frame at Δ to produce a signal with the two distinct time dependences, $\Delta \pm \Omega_{\text{eff}}$ of the second and third terms in Eq. (4).

3. Discussion

3.1. Impact of dynamic phase shifts on DEER measurements

The dynamic phase shifts described here affect DEER measurements in several ways. The most obvious way is the phase shift of the echo. If the spectrometer is tuned with the pump pulse turned off, for instance to record the field swept spectrum, it is necessary to readjust the phase of the receiver or the signal for DEER measurements, which can be problematic with the weak signals at the large values of τ or T required for measurement of long distances. We prefer to record both quadrature channels and phase the spectrum during analysis. The dynamic phase shift is the

same for the modulated DEER signal and for the constant background from isolated radicals or radicals whose partners are not excited as discussed in the next section. Thus the magnitude of the total signal should be maximized by adjustment of the phase of the receiver or by a zero order phase adjustment of both quadrature components of the signal if phase cycling has been used for baseline correction. Misadjustment of the phase does not alter the frequencies in the DEER modulation nor the relative amplitude of the modulation relative to the unmodulated background, and consequently will not change the measured dipolar interaction or distance between radicals. Yet, poor phasing will decrease the amplitude of the signal relative to the noise and produce greater uncertainty in measured distances or increased measurement times.

Optimization of the pump pulse is also affected. The dynamic phase shift depends on B_2, t_p and Δ, so that it is not a simple matter to set the pump pulse for an optimal DEER measurement. It is not sufficient to adjust the pump pulse for minimum echo intensity and assume that the echo reduction is caused by the DEER response. The echo amplitude minimum can arise from the dynamic phase shift and not from achieving an optimal pump pulse of $\gamma B_2 t_p = \pi$. For measurements of distances in pairs of radicals, the pump pulse amplitude merely affects the amplitude of the DEER modulation by affecting the fraction, known as p, of radicals affected by the pump pulse. Since the fraction, p, does not enter into the distance analysis, the major reason for optimizing the pump pulse in measurements on monodisperse pairs of radicals is to maximize sensitivity. However, the fraction, p, is an important parameter in more complicated systems with distributions of distances or in clusters of radicals. The ability to accurately control p by controlling the pump field strength is vital to the correct analysis of the data.

Two common methods of adjusting the pump pulse are to use a strong biradical standard sample or to optimize the spin echo signal measured at the pump frequency. The former method involves changing samples and is impractical for resonators that are strongly perturbed by the sample or have inconvenient sample loading procedures. The later method requires shifting the spectrometer observe frequency, ω_0, to approximately the pump frequency. Then the pump pulse is optimized for some sequence of pulses involving both frequencies so that the resulting signal depends on both amplitudes but only on the phase of the pulses at ω_0. Some groups use a $\pi(\omega_0 - \Delta) - \pi/2(\omega_0) - \pi(\omega_0)$ (inversion-recovery) sequence and adjust for maximum inversion of the echo by the $\pi(\omega_0 - \Delta)$ pulse. We have used a $\pi/2(\omega_0 - \Delta) - \pi/2(\omega_0 - \Delta) - \pi/2(\omega_0)$ (stimulated echo) sequence and optimized the stimulated echo signal with the pulses attenuated by an extra 6 dB. Obviously this approach does not work if the frequency source and receiver for ω_0 cannot be readily adjusted.

The dynamic phase shift provides a new method for setting pump conditions. Under typical conditions for DEER of spin labeled proteins, the frequencies corresponding to signals **1** and **3** of Fig. 2 are easily measured and the value of B_2 calculated from Eq. (5) (or (6)). The optimal $t_p = \pi/\gamma B_2$ can then be set and measurements made without the need to change samples or shift ω_0. If capacitive loading of the pulse programmer channels, as described in the Appendix, is substantial, a common calibration factor determined independently or from the known value of Δ can be used to correct both Δ and B_2.

Under typical DEER measurement conditions, the three spin echoes are not resolved and interference between them can also decrease signal amplitude and sensitivity. The shortest inverting pump pulse usually does not give the greatest sensitivity for DEER. Adjustment of Δ and $t_p = \pi/(\gamma B_2)$ can provide significant improvements in sensitivity by achieving constructive rather than destructive interference of the echoes. Numerical simulations show the maximum signal magnitudes for DEER occurs for $t_p\Delta/(2\pi) = 0.866$ or 1.94 with $\gamma B_2 t_p = \pi$.

3.2. Applicability to interacting radicals

The focus of this paper so far has been the dynamic phase shift in a two-level system appropriate for isolated free radicals. Yet DEER measurements are usually made on multi-level systems consisting of pairs or groups of interacting radicals, each with numerous hyperfine splittings from nuclear spins. We now consider briefly how the dynamic phase shifts affect multi-level systems of typical DEER measurements on interacting radicals using earlier results by Ramsey [6]. A more complete treatment will be the subject of a future paper. We first discuss a four-level system appropriate to DEER measurements on spin-labeled proteins for $\Delta > \gamma B_2 > \omega_{dip}$ and large inhomogeneous broadening of the EPR spectrum, where ω_{dip} is the dipolar splitting. Ramsey (in Eq. (21)) [6] calculated the frequency shift for the dominant echo, **3**, in this limit. There are a total of four EPR-active transitions between the four states of such a coupled radical pair. DEER measurements in this limit detect both EPR transitions of one of the radicals whose transitions are at a frequency $\sim\omega_0$. The other radical in the pair has resonance frequencies centered at ω' which is not necessarily equal to the pump frequency $\omega_0 - \Delta$.

The dipolar interaction splits the EPR line of the observed radical into two lines with a static, dipolar shift of $+\omega_{dip}/2$ and $-\omega_{dip}/2$. During the pump pulse, there are additional shifts [6] for each line (in precession frequency resulting in an echo phase shift) caused by the pump pulse of:

$$\begin{aligned}&\frac{\gamma^2 B_2^2}{2\Delta + \omega_{dip}} + \frac{\gamma^2 B_2^2}{4(\omega' - \omega_0 + \Delta + \omega_{dip}/2)} \\ &\quad - \frac{\gamma^2 B_2^2}{4(\omega' - \omega_0 + \Delta - \omega_{dip}/2)} \\ &\quad = \frac{\gamma^2 B_2^2}{2\Delta + \omega_{dip}} - \frac{\omega_{dip}\gamma^2 B_2^2}{2(\omega' - \omega_0 + \Delta)^2 - \omega_{dip}^2}\end{aligned} \tag{7a}$$

and

$$\frac{\gamma^2 B_2^2}{2\Delta-\omega_{\rm dip}}+\frac{\gamma^2 B_2^2}{4(-\omega'+\omega_0-\Delta+\omega_{\rm dip}/2)} -\frac{\gamma^2 B_2^2}{4(-\omega'+\omega_0-\Delta-\omega_{\rm dip}/2)} =\frac{\gamma^2 B_2^2}{2\Delta-\omega_{\rm dip}}+\frac{\omega_{\rm dip}\gamma^2 B_2^2}{2(\omega'-\omega_0+\Delta)^2-\omega_{\rm dip}^2} \quad (7b)$$

respectively, where the much smaller effects of the counter-rotating circularly polarized components were ignored. Because the dipolar splitting is not resolved in the EPR spectrum for a typical DEER measurement, the measured phase shift is just the average of Eqs. (7a) and (7b). The terms involving ω' shift the dipolar split lines in equal but opposite directions, leaving a net shift of $\gamma^2 B_2^2/(2\Delta)$, which is exactly the shift for a two-level system in the limit of large Δ for echo **3** in Eq. (4) above and in Eq. (12) of Ramsey [6].

The second term on the right hand side of Eq. (7) is not valid when the pump frequency is close to the resonance frequency of the second radical. However, this is precisely the regime that the theory for DEER and for heteronuclear decoupling in NMR have been worked out in detail (see, for example, Maryasov et al. [13,14] and Slichter Chapters 7.20 and 7.21 [15]). When the pump pulse excites the second radical, it produces the well-known DEER modulation with the frequency, $\omega_{\rm dip}$, in addition to the dynamic phase shift of Eq. (4). If it does not excite the second radical, the pump pulse produces only the dynamic phase shift of Eqs. (4) and (7).

The average dynamic phase shift for the observed radical in the pair is the same as for an isolated radical, consequently the DEER signal from a doubly spin labeled protein will have the same optimal phase as for isolated radicals. These same arguments are easily extended to arbitrary numbers of interacting radicals following Ramsey [6] with the result that the dynamic phase shifts caused by the additional radicals are largely self-canceling under typical DEER measurements conditions according to Eq. (7) and converge on the value for an isolated radical because $\omega_{\rm dip}$ averages to zero for typical distributions of distant radicals. This conclusion is supported by the empirical observation that measured dynamic phase shifts are consistent with calculated values for frozen solutions of dilute free radicals, for concentrated radicals in coal and γ-irradiated sugar, and for frozen solutions of doubly spin labeled biomolecules. For the very concentrated radicals in γ-irradiated sugar, we did observe additional frequencies that are sums or differences of those in Eq. (4) in the type of spectra shown in Fig. 5.

Energy levels can be split by hyperfine interactions with nuclei. However, because of the large mismatch between the pump frequency and the nuclear resonance or ENDOR frequencies, electron nuclear interactions produce no significant dynamic phase shift from microwave pulses in the limit that the branching transitions necessary for ESEEM are negligible. The presence of branching transitions requires a more complicated approach that is beyond the scope of this manuscript and potentially introduces ENDOR or ESEEM frequencies into DEER spectra.

4. Conclusions

A strong microwave pulse changes the precession rate of all precessing magnetization in a sample, causing a net shift in the phase of any EPR signal derived from that magnetization. In DEER measurements these dynamic phase shifts caused by the pump pulse appear as: a net phase shift in the detected echo; a shift in the location of the echo by as much as twice the pump pulse width; and a change in the echo shape appearing at the extreme as a splitting of the echo into three echoes. The dynamic phase shifts are easily calculated from the pump pulse width, the pump pulse field and the pump pulse offset frequency, providing a means to calibrate the pump pulse in DEER measurements. The dynamic phase shifts make it problematic to optimize the pump pulse for DEER by minimizing the amplitude of the detected echo.

The dynamic phase shifts are the same for isolated radicals as for pairs or clusters of dipolar coupled radicals and do not vary as the pump pulse is moved within the interval between pulses in the typical DEER measurement. The same spectrometer phase setting is appropriate for DEER measurements on isolated or interacting radicals as long as the pumping pulse width, amplitude and offset frequency remain constant. However, when the pump pulse is removed, overlaps or is placed before the first observing frequency pulse, the magnitude, position and phase of the echo signal change abruptly and such signals cannot be used directly to measure the 'zero-time' DEER modulation.

5. Experimental

All experimental measurements were made using a Bruker EleXsys E580 pulsed X-band EPR spectrometer with integral ELDOR accessory using a Bruker 3 mm Split Ring resonator at room temperature on a roughly 0.5 mm^3 of γ-irradiated sucrose in a capillary tube. The resonator was strongly overcoupled to produce large pump fields at large offsets and to allow use of intense pump pulses with ~π/2 observation pulses. Echoes were generated with the observing frequency set at the resonance frequency of the Split Ring resonator. A 16-step phase cycle was used for most measurements: {x, $-x$, y, $-y$, x, $-x$, y, $-y$, x, $-x$, y, $-y$, x, $-x$, y, $-y$} for the first observation pulse, {x, $-x$, y, $-y$, $-x$, x, $-y$, y, y, $-y$, x, $-x$, $-y$, y, $-x$, x} for the second observation pulse while the two quadrature components of the signal were summed into the a and b channels of the receiver as: {a, $-a$, b, $-b$, a, $-a$, b, $-b$, $-a$, a, $-b$, b, $-a$, a, $-b$, b} and {b, $-b$, $-a$, a, b, $-b$, $-a$, a, $-b$, b, a, $-a$, $-b$, b, a, $-a$}, respectively. This sequence incorporates CYCLOPS and is quite effective in eliminating image peaks in the Fourier Transforms.

Spectra were processed using the Xepr software from Bruker Biospin. Calculations and modeling were performed with Mathematica versions 5.1 and 5.2 and plotted using SigmaPlot 8.0.

Acknowledgments

This work was supported by the National Institutes of Health, GM61904, and by Russian Foundation of Basic Research, Project 06-04-48021a. A.G.M. thanks Battelle Memorial Institute for a Visiting Scientist Fellowship. M.K.B. thanks Marina Benatti and Martina Huber for helpful discussions. A portion of this work was performed at the WR Wiley Environmental Molecular Sciences Laboratory, a national scientific user facility sponsored by the Department of Energy's Office of Biological and Environmental Research and located at Pacific Northwest National Laboratory.

Appendix A. Instrumental considerations

Short electronic pulses are distorted by the impedance of transmission lines in ways that can impact the quantitative measurements described here. In particular, the capacitance of the cables between the pulse programmer and the microwave switches in the spectrometer decreases the width for short pulses and may even cause extremely short pulses to disappear. The ElexSys spectrometer used here is quite good with respect to this capacitive loading, but not completely immune. As a first approximation, the actual pump pulse width, t_p, is related to the pulse width, t_{p0}, set by the PatternJet in the spectrometer used for these measurements by

$$t_p \approx \begin{cases} t_0 + (1+C)t_{p0} & t_{p0} \leqslant 300\ \text{ns} \\ t_0 + C300\ \text{ns} + t_{p0} & t_{p0} > 300\ \text{ns} \end{cases} \quad \text{(A.1)}$$

where t_0 is an intercept (usually slightly negative) that depends on the PatternJet calibration and C is a capacitive loading correction factor for short pulse widths ($C \sim 0.02$–0.03 for the ElexSys system used here). For short pulses, the actual pump pulse width increases faster than the programmed pulse width. Thus, the frequencies in Fig. 5 measured using the programmed pulse width as the time base appear to be 2–3% larger than they really are. The correction factor was measured experimentally by capturing single transients of the DEER pulse with the TM mode of the SpecJet transient recorder for different programmed pulse widths and measuring the width of the magnitude (or absolute value) of the quadrature transients. The pump frequency offset was measured from the Fourier Transform of the difference frequency (in the TM mode) from a broad DEER pulse and agreed with the set Δ independent of frequency offset.

If any of the ridges in Fig. 5 are Fourier Transformed over a range of $t_p < 300$ ns to determine Δ or $\Delta \pm \Omega_{eff}$, the resulting frequencies are scaled by $(1 + C)$ from Eq. (A1) but are easily corrected if either C or the offset frequency is known accurately.

A.1. Observation bandwidth in DEER

The analysis of DEER time-domain spectra requires knowledge or assumptions concerning correlations between the orientations of the two radicals involved [14,16]. When there are correlations, as can easily happen in spin-labeled proteins where the protein provides anisotropic potentials for the labels, any orientation selection in either the pumping or the observation makes the DEER spectra depend on the measurement conditions in both three- and four-pulse DEER. In the ideal case, one would like very narrow pump and observe pulses so that all orientations of the spin-labeled protein would be excited. This would be combined with detection of a single point at the center of the spin echo for maximum detection bandwidth and no orientation selectivity in the detection.

The dynamic phase shift forces some selectivity into the detection under typical DEER measurement conditions where t_p is less than the width of the echo and the three echoes in Fig. 4 are not resolved. The signal consists of three overlapping echoes centered at different times and with different phases, making it impossible to select a single optimal measuring point. Representative frequency responses for a few sets of conditions are illustrated in Fig. A.1. The solid lines in Fig. A.1a and b show the frequency response of the two pulse echo with no dynamic phase shifts for an 8 or 100 ns integration window accurately centered on the echo peak. The receiver phase is set so that the response is entirely in the real (or black) channel and nothing appears in the imaginary (or red) channel. The frequency response is quite broad and positive for the 8 ns integration window of Fig. A.1a and rather narrow and predominantly positive for the 100 ns window in Fig. A.1b. In both cases, the response is an absolutely symmetric $\sin(x)/x$ or $\sin c$ function. These plots of frequency response show only the response caused by the integrator window and by the pump pulse but ignore the resonator and amplifier bandwidth, and the finite excitation pulse widths.

If the integrator window is delayed by 20 ns relative to the echo, there is a considerable change in the frequency response, especially for the narrow integrator windows. The displayed response oscillates in both amplitude and phase across the 200 MHz spectral window. For instance, in Fig. A.1a, electron spins in resonance ($\delta = 0$) with the observing frequency produce the maximum positive response in the real channel (and zero in the imaginary channel) whether or not the integrator window is centered. However, off-resonant spins at $\delta/(2\pi) = \pm 25$ MHz produce nearly an equal but negative response with the off center integrator window! As a result, if measurements are made on an EPR spectrum which is more than 50 MHz wide, the signal from the wings will be subtracted from the signal

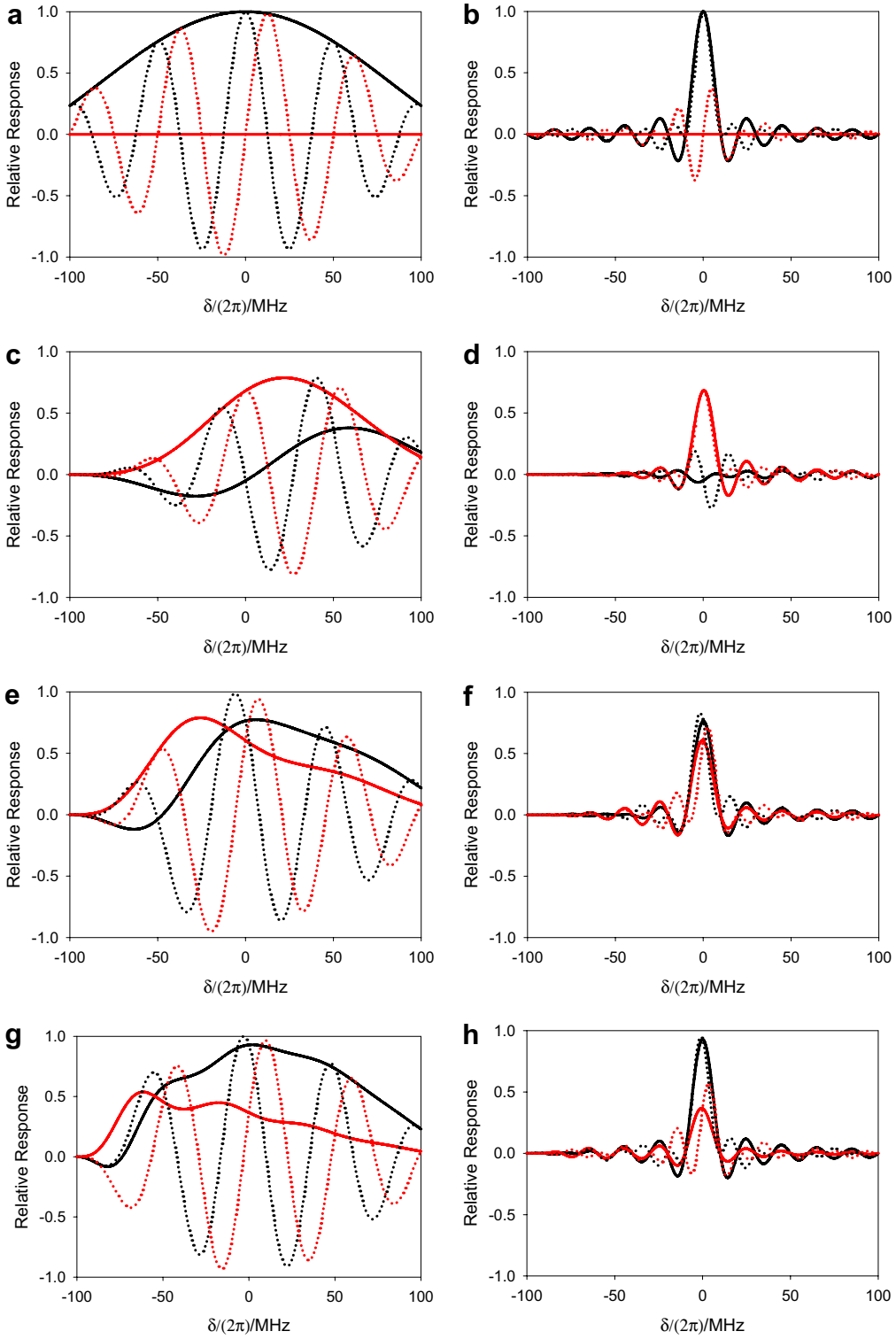

Fig. A.1. Frequency response (relative to the resonance condition at $\delta = 0$) for 3-pulse DEER measurements for various pump fields. Only the effect of the DEER pump pulse and the integrator used in signal capture are considered. The effects of finite observing pulse amplitude and width, resonator Q, signal propagation delays and video amplifier response are specifically excluded. The curves are calculated as the product of Eq. (4) and the Fourier Transform of a square pulse representing the integrator acquisition window and normalized to the peak response in the absence of a pump pulse. The black and red traces represent the real and imaginary components of the quadrature signal phased in the absence of a pump pulse. The solid lines show the response calculated for the integrator window exactly centered on the peak of the electron spin echo while the dotted lines correspond to a delay of the integrator window by 20 ns. The integrator window is 8 ns in plots a, c, e, and g but 100 ns in b, d, f, and h. The first pair, a and b show the response in the absence of a pump pulse, while the other plots are for a pump pulse at $\Delta/2\pi = 100$ MHz with the width set to invert its resonant spins and $\gamma B_2/(2\pi)$ of: 100 MHz, $t_p = 5$ ns for c and d; 50 MHz, $t_p = 10$ ns for e and f; and 25 MHz, $t_p = 20$ ns for g and h.

at the center if the integrator window is incorrectly set by 20 ns. The impact of a poorly positioned integrator window is reduced for a wider integrator window, Fig. A.1b, because a much narrower range of frequencies contribute to the signal.

There are several noticeable changes when a strong pump pulse at $\Delta/(2\pi) = 100$ MHz is applied for DEER measurements, Fig. A.1c and d for $\gamma B_2/(2\pi) = 100$ MHz. One striking change is that the response, for the centered integrator window shown in the solid lines, has largely shifted from the real channel to the imaginary channel because of the dynamic phase shifts. This phase shift is a weak function of frequency. The maximum response shifts by ~25 MHz with the narrow integrator gate but for the wide integrator window there is only a reduction in the amplitude of the peak at $\delta = 0$. Another change is the lack of any response at $\delta/(2\pi) = -100$ MHz which corresponds to spins in resonance with the pump pulse. Their signal is completely suppressed in Fig. A.1c–h because the pump pulse was set precisely to $\gamma B_2 t_p = \pi$.

When the pump field is decreased to 50 or 25 MHz, Fig. A.1e–h, these qualitative changes persist. The peak in the frequency response moves toward δ=0 with some recovery of intensity, while the hole in the response at the pumping frequency becomes narrower. There are also 'ripples' in the signal phase which are even more evident in the solid traces in Fig. A.1e and g. The ripples are a manifestation of the splitting of the signal into three echoes, as in Fig. 4, and make it impossible for a first-order phase correction of the echo signal to make the imaginary channel vanish as in the solid traces of Fig. A.1a and b, making it difficult to reproducibly adjust the phase or correctly position a narrow integrator gate for a broad EPR spectrum. However, the more limited frequency response obtained with a broad integrator window does allow reproducible adjustments but with the risk of appreciable complications in analysis because of the increased orientation selection.

The dynamic phase shifts and amplitude changes produced by the pump pulses in DEER have a definite impact on both data collection and analysis. The use of narrow integrator windows to minimize the potential for orientation selection in the measurement makes the positioning of the integrator window over the echo rather critical. Any mispositioning makes the phase of the signal, and hence the amplitude and sign of any dipolar modulation measured by DEER, vary across the measurement bandwidth. In extreme cases, some parts of the dipolar Pake pattern can become inverted, violating assumptions often made in the analysis of DEER data. Capturing the entire echo with a broad integration window is more reproducible and gives signals that are easier to phase, but the greatly reduced detection bandwidth comes with the potential for strong orientation selectivity which also violates assumptions often made in the analysis of DEER data. Fortunately, DEER studies on SDSL proteins at X-band have been remarkably free of complications from orientation selection so that the integrator window should not be a major concern in this popular application of DEER.

A.2. Three-pulse DEER experiment

The three-pulse DEER experiment, Fig. 1, is performed with two pulses at the observing frequency and one pump pulse. With most spectrometer designs, the pump and observing pulses are amplified in the same amplifier, a TWT or solid state device, operating near saturation. When the two pulses overlap in time, amplifier nonlinearities greatly distort the amplitudes, phases and frequencies of the pulses, preventing measurement of useful data during an experimental deadtime roughly equal to the sum of the pulse widths.

The situation is not much improved on spectrometers that amplify the microwave pulses independently. It is possible to apply undistorted microwave pulses to the sample. However, while the pulses overlap, the spins are subjected to two oscillating fields and evolve non-linearly in that total field in a way that is not the sum of their evolution in the individual fields. Again there is a deadtime that is roughly the sum of the pulse widths. The deadtime is theoretical rather than experimental because there is not an appropriate description of the spin dynamics for overlapping pulses under typical DEER conditions. The missing data from this deadtime can prevent detection of strong dipolar interactions. One approach has been to extrapolate the data back to zero deadtime and match it to the signal amplitude with the pump pulse before both observing pulses. This approach assumes that the echo signal with both observing pulses following the pump pulse corresponds to the DEER signal with no evolution time.

This expectation is clearly not met when dynamic phase shifts are considered. When the pump pulse occurs before the observing pulses, there is no dynamic phase shift. Yet when present after the first observing pulse, the pump pulse always produces a phase shift in the detected echo as shown in Fig. 3. There is a discontinuity in the phase (and usually the amplitude) of the signal as the pump pulse and first observe pulse cross that makes correct phasing of the signal problematic. In addition, the three echoes that form the detected signal interfere destructively to some extent and attenuate the echo signal except for certain combinations of pulse width, offset and B_2 as illustrated in the black trace in Fig. 3 and then only if the pump field is uniform over the entire sample.

In addition to these dynamic phase shift effects, when the pump pulse is placed before the first observe pulse, the pump pulse may decrease the signal amplitude by decreasing the initial M_Z as described by Eq. (1) with $\vec{M}(0) = (0, 0, 1)$. In short, there is generally a discontinuous step in the detected echo signal as the pump and first observe pulse cross. That step is not directly related to the DEER signal within the deadtime of the three-pulse DEER measurement and is not a reliable indication of strong dipolar interactions.

References

[1] A.D. Milov, A.G. Maryasov, Yu.D. Tsvetkov, Pulsed electron double resonance (PELDOR) and its applications in free radicals research, Appl. Magn. Res. 15 (1998) 107–143.
[2] M.K. Bowman, D. Becker, M.D. Sevilla, J.D. Zimbrick, Track structure in DNA irradiated with heavy ions, Radiat. Res. 163 (2005) 447–454.
[3] G. Jeschke, Distance measurements in the nanometer range by pulse EPR, Chemphyschem 3 (2002) 927–932.
[4] G. Jeschke, Determination of the nanostructure of polymer materials by electron paramagnetic resonance spectroscopy, Macromol. Rapid Commun. 23 (2002) 227–246.
[5] F. Bloch, A. Siegert, Magnetic resonance for nonrotating fields, Phys. Rev. 57 (1940) 522–527.
[6] N.F. Ramsey, Resonance transitions induced by perturbations at two or more frequencies, Phys. Rev. 100 (1955) 1191–1194.
[7] C. Wei, A.S.M. Windsor, N.B. Manson, A strongly driven two-level atom revisited: Bloch–Siegert shift versus dynamic stark splitting, J. Phys. B: At. Mol. Opt. Phys. 30 (1997) 4877–4888.
[8] M. Mehring, P. Hofer, A. Grupp, Bloch–Siegert shift, rabi oscillation, and spinor behavior in pulsed electron-nuclear double-resonance experiments, Phys. Rev. A 33 (1986) 3523–3526.
[9] L. Emsley, G. Bodenhausen, Phase-shifts induced by transient Bloch–Siegert effects in NMR, Chem. Phys. Lett. 168 (1990) 297–303.
[10] H. Hatanaka, T. Hashi, Transfer of coherence and effect of level shift caused by two-quantum excitation in a multilevel NMR system, Phys. Rev. B: Condens. Matter 27 (1983) 4095–4109.
[11] V. Weis, M. Bennati, M. Rosay, R.G. Griffin, Solid effect in the electron spin dressed state: a new approach for dynamic nuclear polarization, J. Chem. Phys. 113 (2000) 6795–6802.
[12] A.D. Milov, K.M. Salikhov, M.D. Shirov, Application of Eldor in electron–spin echo for paramagnetic center space distribution in solids, Fiz. Tverd. Tela 23 (1981) 975–982.
[13] A.G. Maryasov, Yu.D. Tsvetkov, Formation of the pulsed electron–electron double resonance (PELDOR) signal in the case of finite amplitude of MW fields, Appl. Magn. Res. 18 (2000) 583–605.
[14] A.G. Maryasov, Y.D. Tsvetkov, J. Raap, Weakly coupled radical pairs in solids: ELDOR in ESE structure studies, Appl. Magn. Res. 14 (1998) 101–113.
[15] C.P. Slichter, Principles of Magnetic Resonance, Springer-Verlag, New York, 1996.
[16] M.K. Bowman, A.G. Maryasov, N.-K. Kim, V.J. DeRose, Visualization of distance distribution from pulsed double electron–electron resonance data, Appl. Magn. Res. 26 (2004) 23–39.